 doi:10.20944/preprints202008.0505.v1

Article

Applying the cracking elements method for analyzing the damaging processes of structures with fissures

Qianqian Dong[1], Jie Wu[2], Zizheng Sun[3], Xiao Yan[4] and Yiming Zhang[2*]

1 College of Aerospace and Civil Engineering, Harbin Engineering University, Harbin, Heilongjiang 150001, China
2 School of Civil and Transportation Engineering, Hebei University of Technology, Beichen District, Tianjin 300401, China
3 School of Qilu Transportation, Shandong University, Jinan 250061, China
4 State Key Laboratory for Geo-mechanics and Deep Underground Engineering, China University of Mining and Technology, 1 Daxue Road, Xuzhou 221116, Jiangsu Province, China
* Correspondence: Yiming.Zhang@hebut.edu.cn; Tel.: +86-022-60435940

Abstract: In this work, the recently proposed cracking elements method (CEM) is used for simulating the damaging processes of structures with initial imperfections. CEM is built in the framework of conventional FEM which is formally like a special type of finite element. The disconnected piecewise cracks are used for representing crack paths. Taking the advantages of CEM that both the initiations and propagations of cracks can be naturally captured, we numerically study the uni-axial compression tests of specimens with multiple joints and fissures, where the cracks may propagate from the tips, or from some other unexpected positions. Though uni-axial compression tests are considered, mainly tensile damage criteria are used in the numerical model. On one hand, the results demonstrate the robustness and effectiveness of the CEM while on the other hand, some drawbacks of the present model are demonstrated, showing the future work.

Keywords: Quasi-brittle material; Cracking elements method; Uni-axial compression tests

1. Introduction

Great engineering practices refer to prediction and prevention of propagation and initiation of cracks in the structures with complex initial imperfection, such as rock mass with joints and concrete structures with early age cracks. When these structures are subjected to complex loading conditions, the existed cracks does not certainly further propagate and the undamaged parts are not naturally safe. For these structures, analytical and empirical analysis are not enough for assuring their safety and durability. Numerical tools with robustness and great efficiency are highly preferable.

With the understanding of continuum-discontinuous theory and developments of computing power, many sophisticated numerical methods are proposed in last decades. These methods can be built in the continuum or discrete framework [1–3], introducing damage degrees [4,5] or crack openings (crack widths) [6,7] as the new freedom degrees. They can localize the damage [8,9] or consider the nonlocal effects [10,11], or even assume the long range forces [12,13]. The crack can be explicitly represented by moving boundaries [14–17] or implicitly embedded for avoiding remeshing [18–21]. The cracked domain can be discretized with elements [6,22,23] or particles [24–26]. In summary, these methods show advantages as well as disadvantages for different problems. Hence, a problem oriented selection procedure would be helpful.

Back to our problem, for analyzing the damaging processes of structures with initial imperfection we need a method capable of capturing initiation as well as propagation of cracks. Since we do not focus on the stress state such as stress intensity factor around specific crack tips, numerical methods using remeshing [15,27,28], nodal enrichment such as eXtended Finite Element Method (XFEM) [18,29–31] and Numerical Manifold Method (NMM) [32–35] are not considered for simplicity. Furthermore, the crack openings are very important for analyzing the durability of structures and the quasi-static loading conditions are considered. Hence, we did not use the damage degree based methods such as phase field method [36–39], mixed mode model [40–43], equivalent lattice models [44–47] and peridynamic based methods [48–51]. Finally, we hope multiple cracks can be efficiently and simultaneously tracked and complicated crack tracking strategies [52,53] can be avoided. The Cracking Elements Method (CEM) [54–57] is the chosen numerical tool.

The CEM is a novel numerical approach belonging to the family of the Strong Discontinuity embedded Approach (SDA) [58–62]. Different from the other SDAs, it introduces disconnected piecewise cracking segments appearing in the center point of each cracked element for representing crack paths, similar to the Cracking Particle Method (CPM) [63–66]. Hence, it does not need to distinguish crack tip element and crack passing element, which naturally captures initiation as well as propagation of cracks. The crack orientation is determined locally, greatly reducing the computing efforts. Moreover, [56] shows that the cracking elements can be treated as a special type of finite element, which is formally like the 9-node quadrilateral element (or 7-node triangular element). Hence, it can be easily implemented in the conventional FEM framework.

In this work, CEM is used for simulating the damaging processes of brittle structures with joints and fissures. The numerically-obtained results are compared the experimental results, where the cracks do not alway propagate from the tips of joints. Especially, uni-axial compression tests are considered while we only use tensile damage criteria in our numerical model. On one hand, agreeable results are obtained in most cases, demonstrating the robustness and applicability of CEM. On the other hand, the differences between the numerical and experimental results will guide us to do our future researches.

The remaining parts of this paper are organized as follows. In Section 2 the constitutive relationship, the formulation of the CEM are presented. The elemental stiffness matrix and residual vector are provided, showing that CEM is very similar to the conventional finite element. The numerical studies are provided in Section 3, comparing to the experimental results. This paper closes with concluding remarks in Section 4.

2. Methods

Since the details of CEM were proposed before in [56,57] with the matrix form, only brief introductions will be provided in this section. By providing the elemental stiffness matrix and residual vector of un-cracked and cracked elements, we will demonstrate the ease of implementing CEM into the FEM framework.

2.1. Traction-separation law

Mixed-mode traction-separation law [67–71] is used in the CEM. Under 2D conditions, the equivalent crack opening is defined as

$$\zeta_{eq} = \sqrt{\zeta_n^2 + \zeta_t^2}, \tag{1}$$

where ζ_n and ζ_t are the crack openings (as unknowns) along the normal and parallel directions, respectively, of the crack path and the corresponding unit vectors are denoted as $\mathbf{n} = \left[n_x, n_y\right]^T$ and

Preprints (www.preprints.org) | NOT PEER-REVIEWED | Posted: 24 August 2020 doi:10.20944/preprints202008.0505.v1

$\mathbf{t} = [t_x, t_y]^T$. Obviously $n_x\, t_x + n_y\, t_y = 0$. The traction components along $\mathbf{n}$ and $\mathbf{t}$, namely, T_n and T_t, respectively, are obtained as

$$T_n = T_{eq}\frac{\zeta_n}{\zeta_{eq}},\ T_t = T_{eq}\frac{\zeta_t}{\zeta_{eq}}$$

with

$$T_{eq}\left(\zeta_{eq}\right) = \begin{cases} TL\left(\zeta_{eq}\right) = f_t \exp\left(-\dfrac{f_t}{G_f}\zeta_{eq}\right), & \text{loading,} \\ TU\left(\zeta_{eq}\right) = \dfrac{T_{mx}}{\zeta_{mx}}\zeta_{eq}, & \text{unloading/reloading,} \end{cases} \tag{2}$$

where f_t is the uni-axial tensile strength, G_f is the fracture energy, ζ_{mx} is the maximum opening the crack has ever experienced, and $T_{mx} = TL\left(\zeta_{mx}\right)$ is the corresponding traction. The traction-separation law indicates that CEM is consistent with the conventional cohesive zone model, as a crack opening-based model but not a damge degree-based model.

Correspondingly, the relationship between the traction differentials dT_n and dT_t and the crack openings ζ_n and ζ_t are described by

$$\mathbf{D}\begin{bmatrix} d\zeta_n \\ d\zeta_t \end{bmatrix} = \begin{bmatrix} dT_n \\ dT_t \end{bmatrix}, \tag{3}$$

with

$$\mathbf{D} = -\frac{T_{eq}}{\zeta_{eq}}\begin{bmatrix} \dfrac{\zeta_n^2}{\zeta_{eq}^2} + \dfrac{f_t\,\zeta_n^2}{G_f\,\zeta_{eq}} - 1 & \dfrac{\zeta_n\,\zeta_t}{\zeta_{eq}^2} + \dfrac{f_t\,\zeta_n\,\zeta_t}{G_f\,\zeta_{eq}} \\ \dfrac{\zeta_n\,\zeta_t}{\zeta_{eq}^2} + \dfrac{f_t\,\zeta_n\,\zeta_t}{G_f\,\zeta_{eq}} & \dfrac{\zeta_t^2}{\zeta_{eq}^2} + \dfrac{f_t\,\zeta_t^2}{G_f\,\zeta_{eq}} - 1 \end{bmatrix} \text{ for loading,}$$

and

$$\mathbf{D} = \frac{T_{mx}}{\zeta_{mx}}\begin{bmatrix} 1 & 0 \\ 0 & 1 \end{bmatrix} \text{ for unloading/reloading,} \tag{4}$$

in which $\mathbf{D}$ obviously remains symmetric.

On the other hand, some other types of the traction-separation law, such as linear, bilinear and hyperbolic, can also be applied but have not yet been attempted. We prefer the exponential law because i) it only needs two parameters: f_t and G_f both of which have strong physical meanings and can be experimentally obtained in the standard tests; ii) it has C^∞ continuity, make $\mathbf{D}$ very simple.

2.2. Elemental formulation

In our early work such as [54,55], we focused on the deduction processes of CEM framework by introducing the strain localization [72,73] and Enhanced Assumed Strains (EAS) [74–76] in which process many complicated tensors are assumed. This on one hand paved the basis of this method which on the other hand reduced the readability. In this work, only 2D condition is considered. We use Voigt notation for representing all second- and fourth-order tensors with corresponding vector and matrix forms [77]. Moreover, from a practical point of view we will directly provide the elemental formulation of un-cracked and cracking element for comparisons.

Firstly, for nonlinear analysis the standard Newton-Raphson (N-R) iteration procedure is used. The global vector of freedom degrees are represented with symbol $\mathbf{U} = \bigcup \mathbf{U}^{(e)}$, where $\bigcup(\cdot)$ denotes the assemblage of elemental matrix or vector to the global form. Considering the load step i in iteration step j, the following equation is introduced:

$$\mathbf{U}_{i,j} = \underbrace{\mathbf{U}_{i-1} + \Delta\mathbf{U}_{j-1}}_{\text{known}} + \underbrace{\Delta\Delta\mathbf{U}}_{\text{unknown}}, \tag{5}$$

Preprints (www.preprints.org) | NOT PEER-REVIEWED | Posted: 24 August 2020 doi:10.20944/preprints202008.0505.v1

Then, the linearized balance equation is represented as

$$\mathbf{K}_{j-1}\ \Delta\Delta\mathbf{U} = \mathbf{R}_{j-1}, \tag{6}$$

where $\mathbf{K}_{j-1}$ is the global stiffness matrix, with $\mathbf{K} = \bigcup \mathbf{K}^{(e)}$. $\mathbf{R}_{j-1}$ is the residual vector, with $\mathbf{R} = \bigcup \mathbf{R}^{(e)}$. $\mathbf{R}_{j-1}$ is a function of $\left(\mathbf{U}_{i-1} + \Delta\mathbf{U}_{j-1}\right)$. Then for the elemental stiffness matrix $\mathbf{K}^{(e)}$ and the residual vector $\mathbf{R}^{(e)}$ of un-cracked element and cracking element, we have

2.2.1. Un-cracked element

For an un-cracked element e, its unknown vector $\mathbf{U}^{(e)} = [\mathbf{u}_1 \cdots \mathbf{u}_n]^T$ in which n is the node number. Its shape function is denoted as $\mathbf{N}^{(e)}$ with $\mathbf{u}(\mathbf{x}) = \mathbf{N}^{(e)}(\mathbf{x})\ \mathbf{U}^{(e)}$ and its B matrix is corresponding denoted as $\mathbf{B}^{(e)} = \nabla\mathbf{N}^{(e)}$. When ignoring the material nonlinear effects, its elemental stiffness matrix $\mathbf{K}^{(e)}$ is obtained as

$$\mathbf{K}_{j-1}^{(e)} = \mathbf{K}^{(e)} = \int \left(\mathbf{B}^{(e)}\right)^T\ \mathbf{C}^{(e)}\ \mathbf{B}^{(e)}\ d(e), \tag{7}$$

where $\mathbf{C}^{(e)}$ is the matrix form of the elastic tensor. Its residual vector at iteration step $j-1$, $\mathbf{R}_{j-1}^{(e)}$ is obtained as

$$\mathbf{R}_{j-1}^{(e)} = \mathbf{F}^{(e)} - \mathbf{K}^{(e)}\ \left(\mathbf{U}_{i-1} + \Delta\mathbf{U}_{j-1}\right), \tag{8}$$

where $\mathbf{F}^{(e)}$ is the loading forces on corresponding nodes. Because $\mathbf{K}^{(e)}$ will not change during the iteration, only one iteration step is needed for convergence.

2.2.2. Cracking element

On the other hand, for cracking element, its unknown vector is defined as $\mathbf{U}^{(e)} = [\mathbf{u}_1 \cdots \mathbf{u}_n, \zeta_n, \zeta_t]^T$. Its B matrix is extended to

$$\mathbf{B}^{(e)} = \left[\nabla\mathbf{N}^{(e)}, \mathbf{B}_\zeta\right], \tag{9}$$

where $\mathbf{N}^{(e)}$ is the original shape function and

$$\mathbf{B}_\zeta^{(e)} = -\left(l_c^{(e)}\right)^{-1} \begin{bmatrix} n_x^{(e)} \cdot n_x^{(e)} & n_x^{(e)} \cdot t_x^{(e)} \\ n_y^{(e)} \cdot n_y^{(e)} & n_y^{(e)} \cdot t_y^{(e)} \\ 2\, n_x^{(e)} \cdot n_y^{(e)} & n_x \cdot t_y^{(e)} + n_y^{(e)} \cdot t_x^{(e)} \end{bmatrix}, \tag{10}$$

where the element-dependent parameter $l_c^{(e)}$ is obtained as $l_c^{(e)} = V^{(e)}\ /\ A^{(e)}$, where $V^{(e)}$ denotes the volume of element e and $A^{(e)}$ stands for the surface area of an equivalent crack parallel to the real crack. Actually l_c corresponds to the classic characteristic length [78,79]. Here, the determination of $A^{(e)}$ for 8-node quadrilateral (Q8) and 6-node triangular (T6) element is slightly different insofar as the equivalent crack passes through the center point of Q8 but through the midpoint of one edge of T6; see Figure 1. More details can be found in [56,57]. Its elemental stiffness matrix $\mathbf{K}^{(e)}$ can be obtained as

$$\mathbf{K}_{j-1}^{(e)} = \int \left(\mathbf{B}^{(e)}\right)^T\ \mathbf{C}^{(e)}\ \mathbf{B}^{(e)}\ d(e) + \begin{bmatrix} \mathbf{0} & \mathbf{0} \\ \mathbf{0} & A^{(e)}\ \mathbf{D}^{(e)} \end{bmatrix}. \tag{11}$$

Because the crack orientation ($\mathbf{n}$) and crack openings will change during the iteration. $\mathbf{K}_{j-1}^{(e)}$ of cracking element is not constant. Its residual vector at iteration step $j-1$, $\mathbf{R}_{j-1}^{(e)}$ is obtained as

$$\mathbf{R}_{j-1}^{(e)} = \begin{bmatrix} \mathbf{F}^{(e)} \\ -A^{(e)}\ \mathbf{T}^{(e)} \end{bmatrix} - \mathbf{S}_{j-1}^{(e)}\ \left(\mathbf{U}_{i-1} + \Delta\mathbf{U}_{j-1}\right). \tag{12}$$

Preprints (www.preprints.org) | NOT PEER-REVIEWED | Posted: 24 August 2020 doi:10.20944/preprints202008.0505.v1

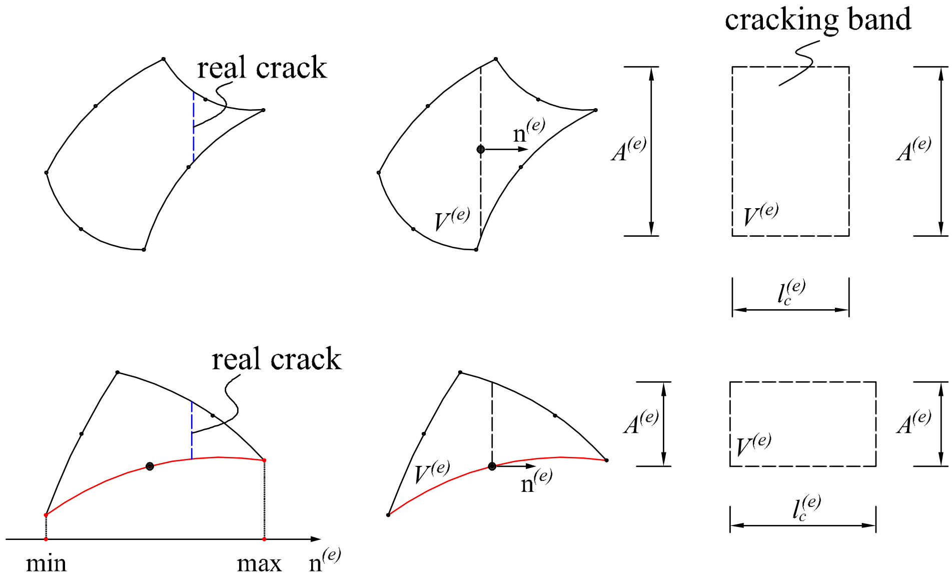

Figure 1. Relationships between l_c, $V^{(e)}$ and $A^{(e)}$ of Q8 and T6

where $\mathbf{T}^{(e)} = \left[T_n^{(e)}, T_t^{(e)}\right]^T$ (see Eq. 2) and $\mathbf{S}_{j-1}$ is a designed unsymmetrical matrix as

$$\mathbf{S}_{j-1} = \begin{bmatrix} \int \left(\nabla\mathbf{N}^{(e)}\right)^T \mathbf{C}^{(e)} \left(\widehat{\nabla\mathbf{N}^{(e)}}\right) d(e) & \int \left(\nabla\mathbf{N}^{(e)}\right)^T \mathbf{C}^{(e)}\, \mathbf{B}_\zeta^{(e)} d(e) \\ V^{(e)} \left(\mathbf{B}_\zeta^{(e)}\right)^T \mathbf{C}^{(e)} \left(\widehat{\nabla\mathbf{N}^{(e)}}\right) & V^{(e)} \left(\mathbf{B}_\zeta^{(e)}\right)^T \mathbf{C}^{(e)}\, \mathbf{B}_\zeta^{(e)} \end{bmatrix}, \tag{13}$$

91 where $\widehat{\nabla\mathbf{N}^{(e)}}$ is value of $\nabla\mathbf{N}^{(e)}$ at the center point of element e.

In summary, the elemental formulations of un-cracked element and cracking element are very similar. Once an un-crack element becomes cracking element, by replacing its elemental stiffness matrix and residual vector provided in Eqs. 7 and 8 into the new form provided in Eqs. 11 and 12, the cracks can be captured. Formally, the quadrilateral cracking element is similar to 9-node quadrilateral element (transformed from Q8) and the triangular cracking element is similar to 7-node triangular element (transformed from T6). The displacement freedom degrees of the center point is now used for representing the normal and shear crack openings.

2.3. Determination of $\mathbf{n}$, crack propagation and initiation

A local criterion is firstly proposed in [54] for determining $\mathbf{n}$, that $\mathbf{n}$ is assumed to be the first eigenvector of the total strain $\widehat{\boldsymbol{\varepsilon}^{(e)}}$, which is determined by

$$\widehat{\boldsymbol{\varepsilon}^{(e)}} = \begin{bmatrix} \widehat{\varepsilon}_x^{(e)} \\ \widehat{\varepsilon}_y^{(e)} \\ \widehat{\gamma}_{xy}^{(e)} \end{bmatrix} = \widehat{\nabla\mathbf{N}^{(e)}} \begin{bmatrix} \mathbf{u}_1 \\ \vdots \\ \mathbf{u}_n \end{bmatrix}, \tag{14}$$

which is independent of ζ_n and ζ_t. After solving the eigenvalue and eigenvector, we obtain

$$\begin{gathered}\left[\begin{array}{c} n_x^{(e)} \\ n_y^{(e)} \end{array}\right] = \left[\begin{array}{c} a \;/\; \sqrt{a^2+b^2} \\ b \;/\; \sqrt{a^2+b^2} \end{array}\right] \\ \text{where} \\ a = \frac{\widehat{\gamma}_{xy}^{(e)}}{2} \\ b = \frac{\widehat{\varepsilon}_y^{(e)} - \widehat{\varepsilon}_x^{(e)} + \sqrt{\left(\widehat{\varepsilon}_x^{(e)} - \widehat{\varepsilon}_y^{(e)}\right)^2 + \left(\widehat{\gamma}_{xy}^{(e)}\right)^2}}{2}.\end{gathered} \tag{15}$$

100 In the framework of CEM, the element will experience cracking one after another. Crack propagation is always checked first; then, crack initiation is considered. This procedure is based on an idea that when the extensions of the existed cracks cannot fully release the extra stresses, new cracks will appear. This procedure was used for capture the dynamic crack propagation in [55], showing robustness as well.

Firstly an index $\phi_{RK}^{(e)}$ is introduced as

$$\phi_{RK}^{(e)} = \left[\begin{array}{c} n_x^{(e)} \cdot n_x^{(e)} \\ n_y^{(e)} \cdot n_y^{(e)} \\ 2\, n_x^{(e)} \cdot n_y^{(e)} \end{array}\right]^T \mathbf{C}^{(e)} \left[\begin{array}{c} \widehat{\varepsilon}_x^{(e)} \\ \widehat{\varepsilon}_y^{(e)} \\ \widehat{\gamma}_{xy}^{(e)} \end{array}\right] - f_t^{(e)} \tag{16}$$

Then, following computing procedure is conducted

1. The un-cracked domain is divided into two sub-domains as i) propagation domain, ii) crack root domain, base on a simple rule: when the elements share at least one edge with the cracking elements, they belong to the propagation domain, otherwise they are in the crack root domain. Obviously in the beginning the whole domain is crack root domain;
2. Find $\left\{\max\left\{\phi_{RK}^{(e)}\right\}\right\}$ in the propagation domain. If $\left\{\max\left\{\phi_{RK}^{(e)}\right\}\right\} > 0$, the element becomes cracking element, then two sub-domains will be updated, the N-R iteration will be run and this step will be conducted again. If $\left\{\max\left\{\phi_{RK}^{(e)}\right\}\right\} \leq 0$, do the next step;
3. Find $\left\{\max\left\{\phi_{RK}^{(e)}\right\}\right\}$ in the crack root domain. If $\left\{\max\left\{\phi_{RK}^{(e)}\right\}\right\} > 0$, the element becomes cracking element, then two sub-domains will be updated, the N-R iteration will be run and step 2 will be conducted again. If $\left\{\max\left\{\phi_{RK}^{(e)}\right\}\right\} \leq 0$, this loading step is considered to converge.

A detained flowchart can be found in [56].

3. Numerical investigations

The plane stress condition is considered for all the examples provided in this section.

3.1. Sandstone containing three pre-existing fissures

The first example is the uni-axial compression tests of sandstone specimens with three fissures, which was experimentally studied in [80]. This example was numerically studied by bond-based peridynamic model in [81], as a damage degree based model. To the best of our knowledge, this example has not been numerically studied by a crack-opening based model in published literatures. The model, material, and discretization are shown in Figure 2. The meshes will slightly change with different setup of the fissures. Although the specimens are subjected to compression loading, they experience mainly tensile damages.

The force-displacement curves and the maximum vertical loads comparing to the experimental results are show in Figure 3. In the force-displacement curves, oscillations correspond to the connecting

Preprints (www.preprints.org) | NOT PEER-REVIEWED | Posted: 24 August 2020 doi:10.20944/preprints202008.0505.v1

of different fissures by propagating cracks. Furthermore, considering the maximum vertical loads, similar to the experimental results, we found the position of the fissure No.3 has limited influences on the maximum σ_y. The crack openings plots comparing to the experimental results are shown in Figures 4 to 7, indicating that CEM is capable of simulating multiple crack propagations and the connections of different fissures.

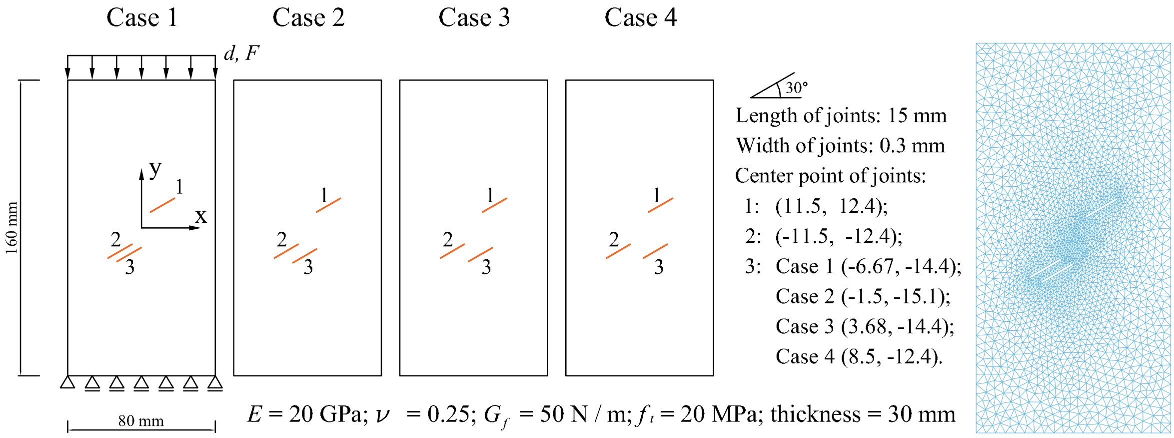

Figure 2. Sandstone containing three pre-existing fissures: model, material, and discretization

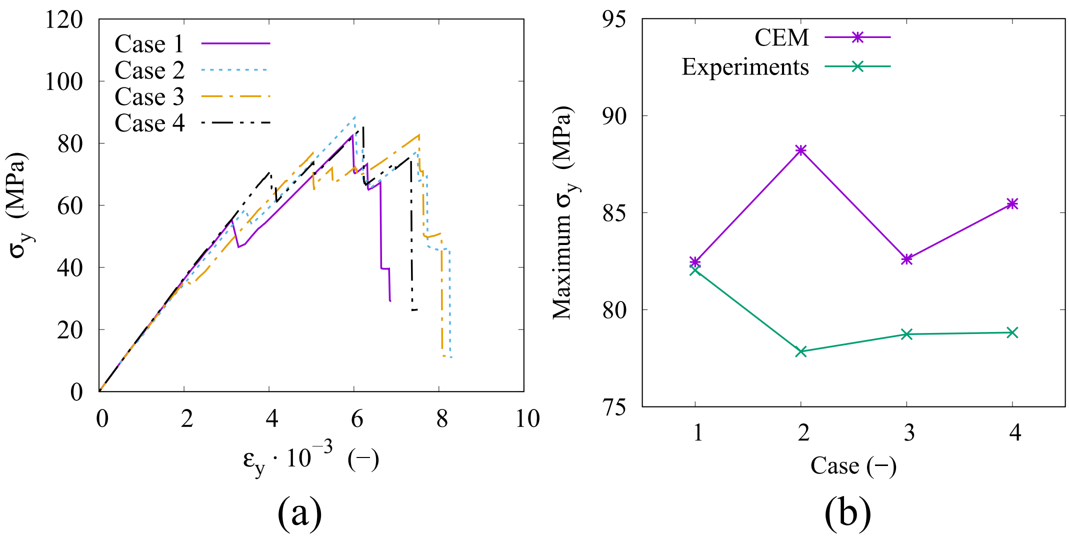

Figure 3. Sandstone containing three pre-existing fissures: (a) force-displacement curves, (b) maximum vertical loads comparing to the experimental results provided in [80]

3.2. 3D-printed materials with two intermittent fissures

The second example is the uni-axial compression tests of 3D-printed materials with two intermittent fissures, which was experimentally studied in [82]. The model, material, and discretization are shown in Figure 8, with width of fissures: 0.3 mm. It can be found that only elastic modulus, Poisson's ratio, fracture energy, and uni-axial tensile strength are needed in our model.

The force-displacement curves and the maximum vertical loads comparing to the experimental results are show in Figure 9. Generally the numerically-obtained results are agreeable. Parts of the crack openings plots comparing to the experimental results are shown in Figures 10 to 13. It can be found that in most cases of the simulations, the two fissures are not connected by the propagating cracks, which is not very agreeable to the experimental results. We attribute the differences to two reasons: i) the shearing damage is not accounted in the present model and ii) the free horizontal boundary conditions on the top and bottom sides of the specimens cannot be assured in the experimental investigations.

Preprints (www.preprints.org) | NOT PEER-REVIEWED | Posted: 24 August 2020 doi:10.20944/preprints202008.0505.v1

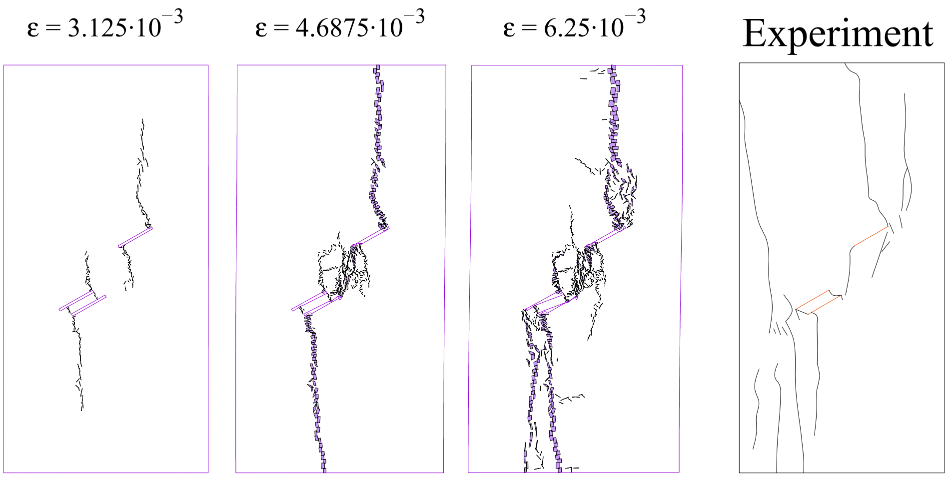

Figure 4. Sandstone containing three pre-existing fissures (Case 1): crack openings plots (deformation scale 1:1) comparing to the experimental results provided in [80]

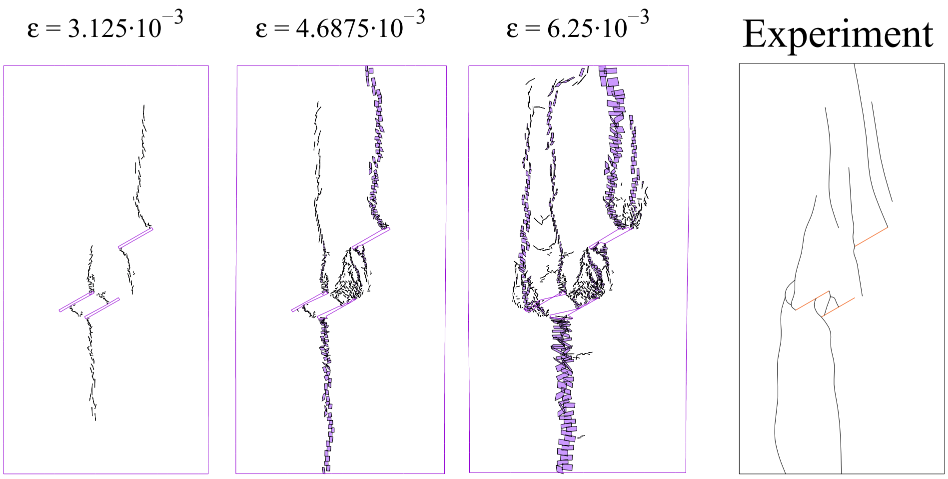

Figure 5. Sandstone containing three pre-existing fissures (Case 2): crack openings plots (deformation scale 1:1) comparing to the experimental results provided in [80]

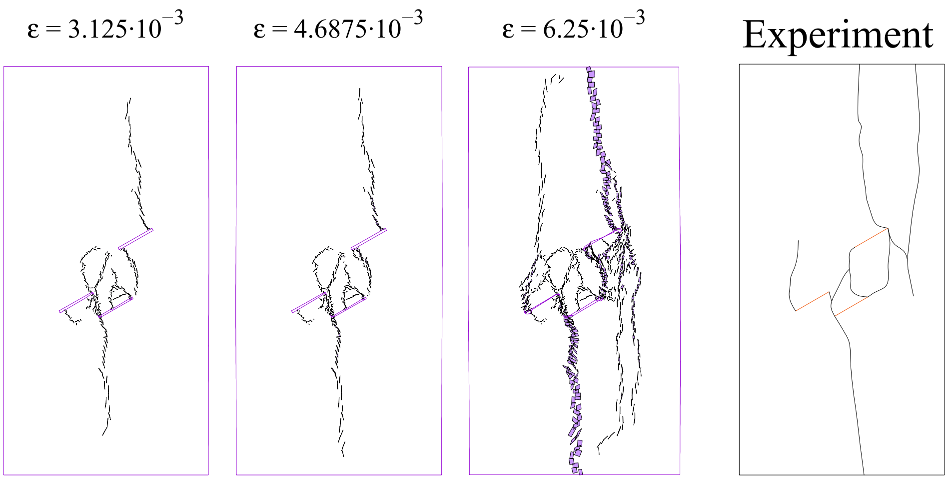

Figure 6. Sandstone containing three pre-existing fissures (Case 3): crack openings plots (deformation scale 1:1) comparing to the experimental results provided in [80]

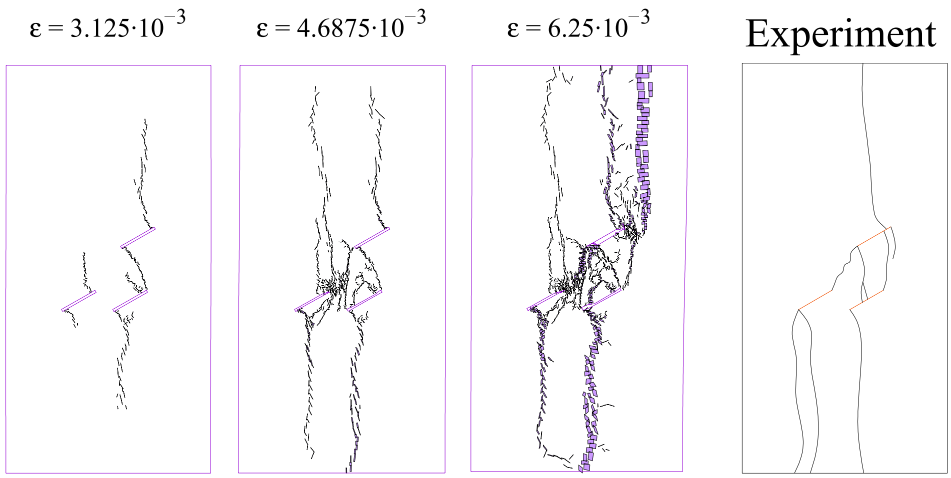

Figure 7. Sandstone containing three pre-existing fissures (Case 4): crack openings plots (deformation scale 1:1) comparing to the experimental results provided in [80]

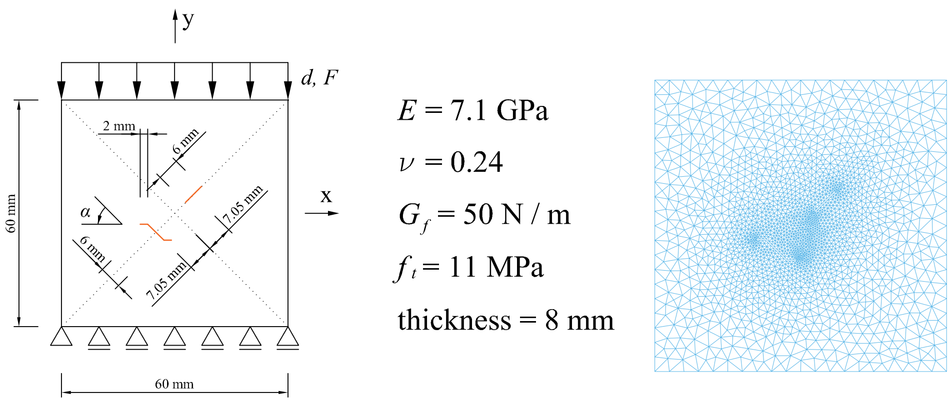

Figure 8. 3D-printed materials with two intermittent fissures: model, material and meshes

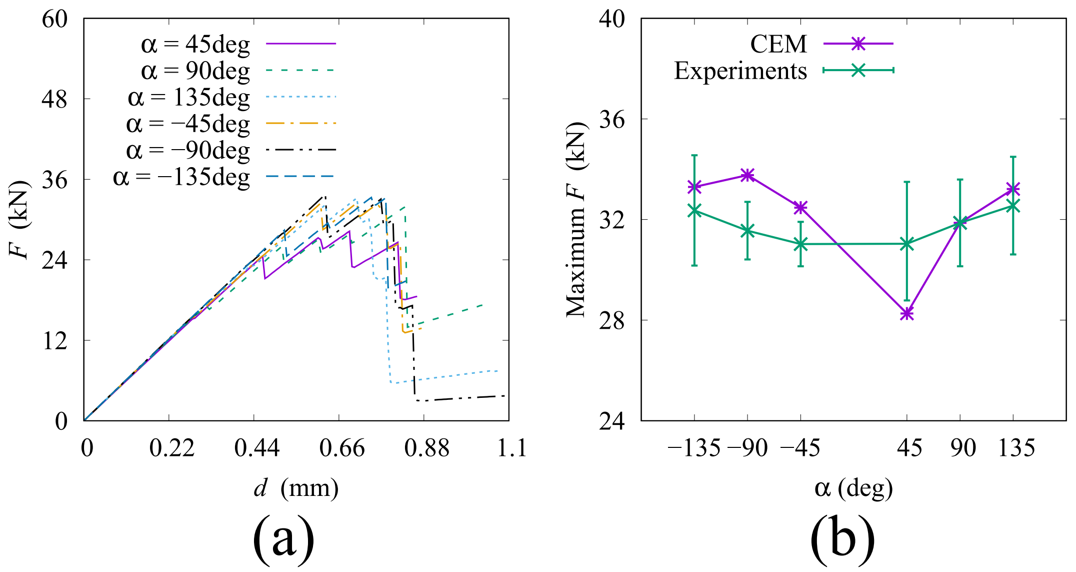

Figure 9. 3D-printed materials with two intermittent fissures: (a) force-displacement curves, (b) maximum vertical loads comparing to the experimental results provided in [82]

Preprints (www.preprints.org) | NOT PEER-REVIEWED | Posted: 24 August 2020 doi:10.20944/preprints202008.0505.v1

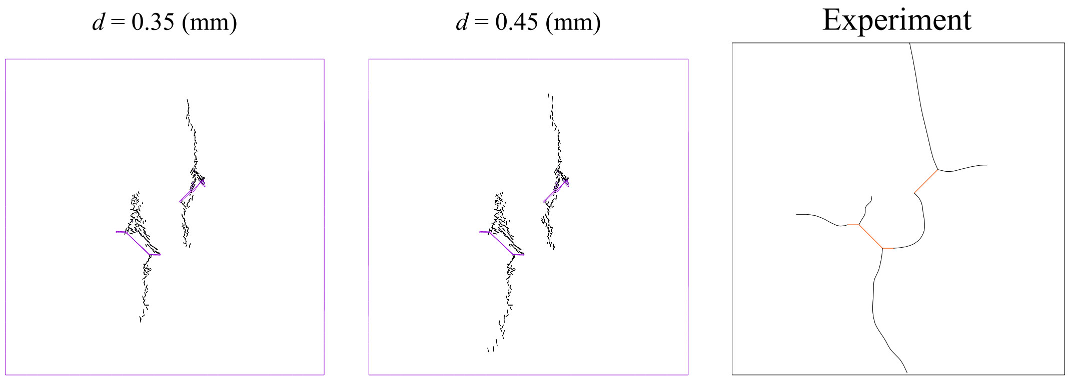

Figure 10. 3D-printed materials with two intermittent fissures ($\alpha = 45°$): crack openings plots (deformation scale 1:1) comparing to the experimental results provided in [82]

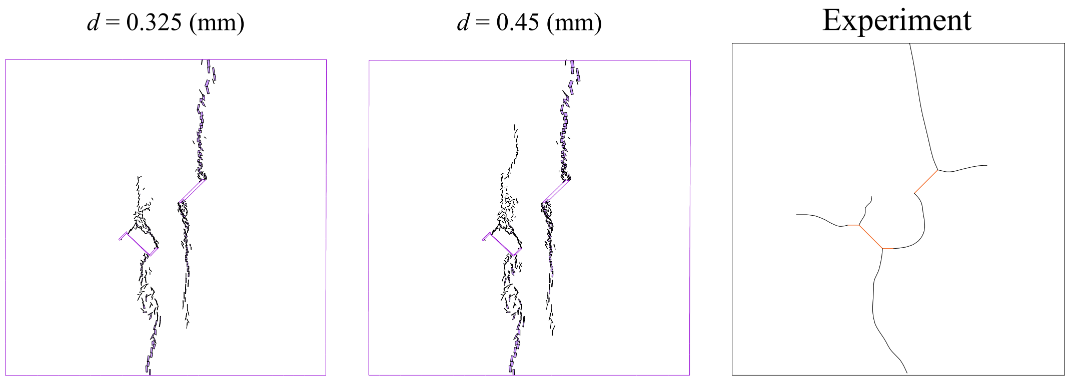

Figure 11. 3D-printed materials with two intermittent fissures ($\alpha = 90°$): crack openings plots (deformation scale 1:1) comparing to the experimental results provided in [82]

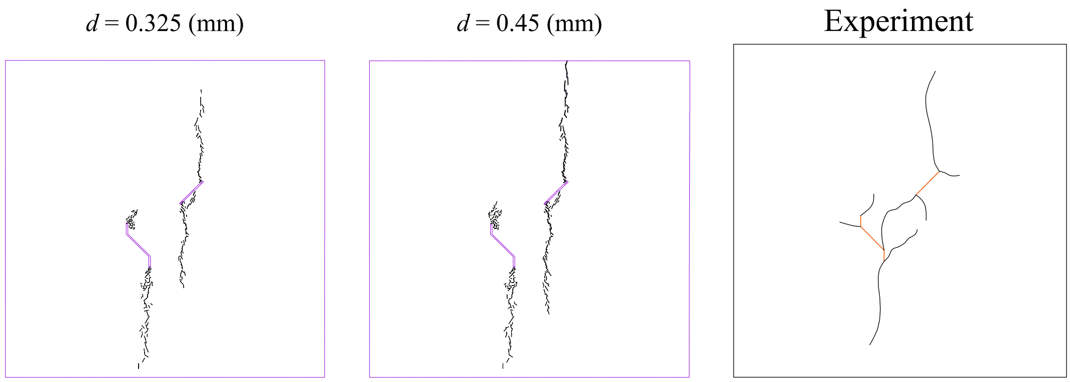

Figure 12. 3D-printed materials with two intermittent fissures ($\alpha = -45°$): crack openings plots (deformation scale 1:1) comparing to the experimental results provided in [82]

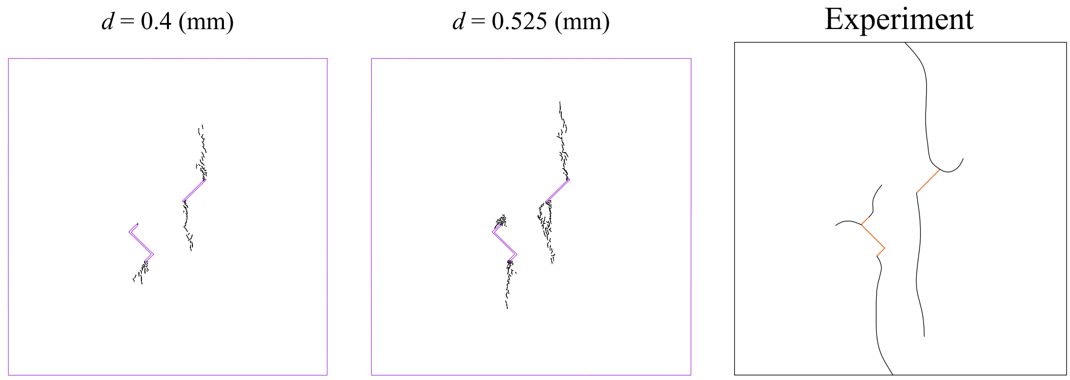

Figure 13. 3D-printed materials with two intermittent fissures ($\alpha = -90°$): crack openings plots (deformation scale 1:1) comparing to the experimental results provided in [82]

3.3. Rock-like materials with nine parallel fissures

The third example is the uni-axial compression tests of rock-like brittle materials with nine parallel fissures, which was experimentally studied in [83]. The model, material, and discretization are shown in Figure 14. Five cases regarding different values of θ are considered as $\theta = 15°$, $\theta = 30°$, $\theta = 45°$, $\theta = 60°$, and $\theta = 75°$.

We only compare the numerically and experimentally obtained results of crack opening (crack paths). The crack openings plots are shown in Figure 15. Comparing to the experimental results shown in Figure 16, it can be found that the tensile induced cracks are successfully captured by CEM, including some branching and nucleation of cracks. Especially for the cases with small values of θ, the tensile damages are dominate. However, some drawbacks of our model are indicated as

- When the fissures are explicitly modeled, the contacts between the two surfaces of fissures shall be taken into account. When taking advantage of CEM, implicit modeling of fissures shall be developed. In other words, fissure shall be treated as embedded cracks, where the closing of cracks can be modeled easier.
- With the increasing of θ, shearing damages become dominant. For shearing damages, orientation of the shear bonds depend on the properties of the acoustic tensor [84,85]. Corresponding shearing damage criteria and model shall be developed and implemented in the CEM.

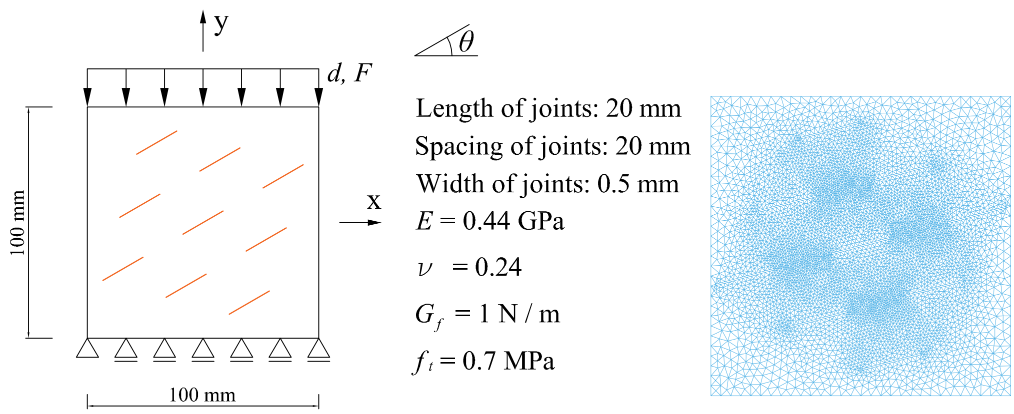

Figure 14. Rock-like materials with nine parallel fissures: model, material and meshes

4. Conclusions and outlooks

In this work, the damage processes of structures with fissures are analyzed with the Crack Elements Method (CEM). Uni-axial compression tests are considered while tensile damage model is

Preprints (www.preprints.org) | NOT PEER-REVIEWED | Posted: 24 August 2020 doi:10.20944/preprints202008.0505.v1

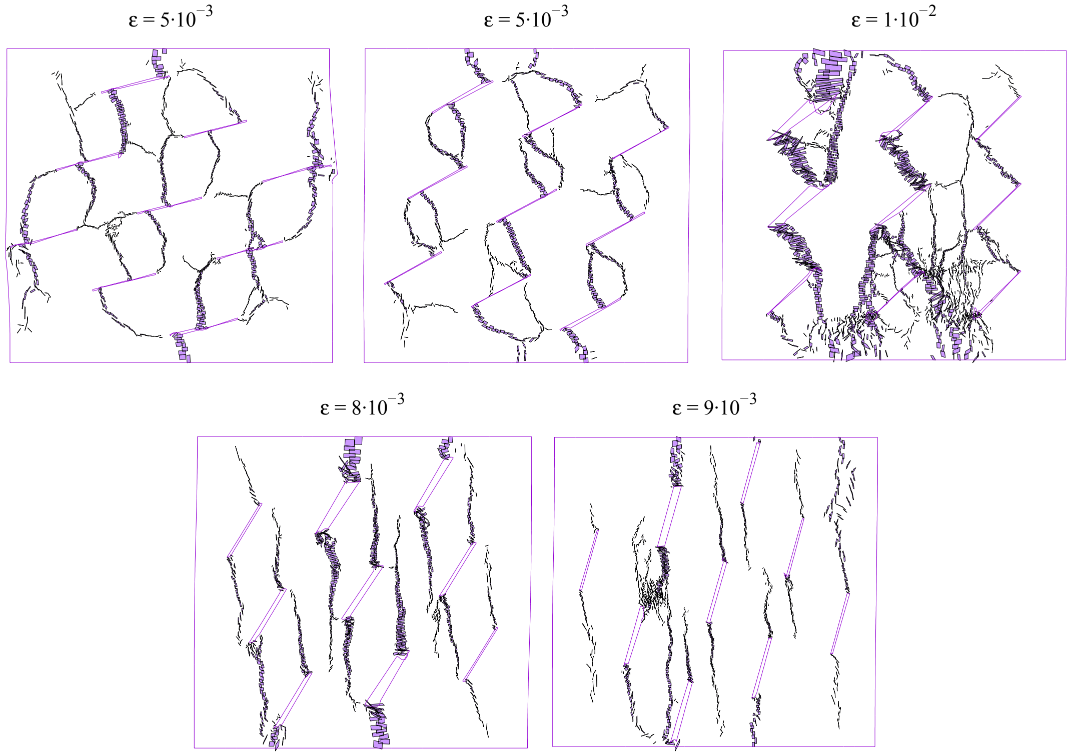

Figure 15. Rock-like materials with nine parallel fissures: numerically-obtained crack openings plots (deformation scale 1:1)

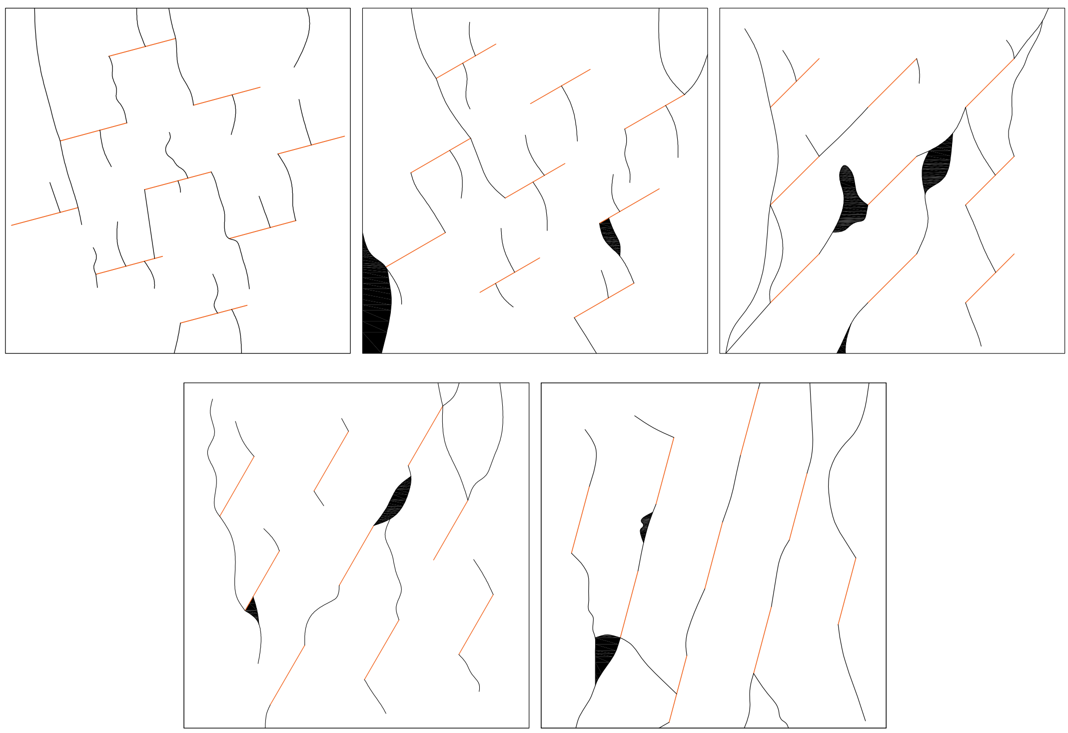

Figure 16. Rock-like materials with nine parallel fissures: experimentally-obtained crack paths (the shadows indicate broken surfaces)

used in the model. For such structures and loading conditions, the crack may propagate from the tips or some other positions of the fissures. The cracks will connect several fissures or propagate independently. Sometimes, new cracks may initiate from unexpected positions. The results demonstrate the advantages of the CEM, which is capable of capturing both initiations and propagations of cracks. On the other hands, some drawbacks of the present model are also revealed, indicating our future work about the CEM, including the implicit modeling of the fissures and the implementation of shearing damage models.

Author Contributions: "Conceptualization, Yiming Zhang; Methodology, Yiming Zhang; Software, Yiming Zhang, Xiao Yan; Validation, Qianqian Dong, Jie Wu, Zizheng Sun; Formal Analysis, Qianqian Dong, Jie Wu; Investigation, Qianqian Dong, Jie Wu Zizheng Sun; Data Curation, Qianqian Dong, Jie Wu; Writing-Original Draft Preparation, Yiming Zhang, Xiao Yan; Writing—Review & Editing, Yiming Zhang; Visualization, Qianqian Dong, Zizheng Sun, Xiao Yan; Supervision, Yiming Zhang; Project Administration, Yiming Zhang; Funding Acquisition, Yiming Zhang"

Funding:

The authors wish to acknowledge the financial support from the National Natural Science Foundation of China (Project No. 51808185, 41807277, 51809069).

Conflicts of Interest: The authors declare no conflict of interest.

Abbreviations

The following abbreviations are used in this manuscript:

CEM	Cracking Elements Method
FEM	Finite Element Method
XFEM	eXtended Finite Element Method
NMM	Numerical Manifold Method
SDA	Strong Discontinuity embedded Approach
CPM	Cracking Particle Method
EAS	Enhanced Assumed Strains

References

1. R. de Borst, J. J. Remmers, A. Needleman, and M.-A. Abellan, "Discrete vs smeared crack models for concrete fracture: bridging the gap," *International Journal for Numerical and Analytical Methods in Geomechanics*, vol. 28, pp. 583–607, 2004.
2. J.-Y. Wu, J.-F. Qiu, V. P. Nguyen, T. K. Mandal, and L.-J. Zhuang, "Computational modeling of localized failure in solids: Xfem vs pf-czm," *Computer Methods in Applied Mechanics and Engineering*, vol. 345, pp. 618 – 643, 2019.
3. Y. Zhang, Z. Gao, Y. Li, and X. Zhuang, "On the crack opening and energy dissipation in a continuum based disconnected crack model," *Finite Elements in Analysis and Design*, vol. 170, 2020. doi: 10.1016/j.finel.2019.103333.
4. M. Geers, R. D. Borst, and R. Peerlings, "Damage and crack modeling in single-edge and double-edge notched concrete beams," *Engineering Fracture Mechanics*, vol. 65, pp. 247–261, 2000.
5. S. Saloustros, L. Pelà, and M. Cervera, "A crack-tracking technique for localized cohesive–frictional damage," *Engineering Fracture Mechanics*, vol. 150, pp. 96–114, 2015.
6. J. Oliver, I. Dias, and A. Huespe, "Crack-path field and strain-injection techniques in computational modeling of propagating material failure," *Computer Methods in Applied Mechanics and Engineering*, vol. 274, pp. 289–348, 2014.
7. S. Saloustros, L. Pelà, M. Cervera, and P. Roca, "Finite element modelling of internal and multiple localized cracks," *Computational Mechanics*, vol. 59, pp. 299–316, 2017.
8. F. Armero and K. Garikipati, "An analysis of strong discontinuities in multiplicative finite strain plasticity and their relation with the numerical simulation of strain localization in solids," *International Journal of Solids and Structures*, vol. 33, pp. 2863–2885, 1996.

9. R. I. Borja, "Finite element simulation of strain localization with large deformation: capturing strong discontinuity using a Petrov-Galerkin multiscale formulation," *Computer Methods in Applied Mechanics and Engineering*, vol. 191, pp. 2949–2978, 2002.
10. C. Giry, F. Dufour, and J. Mazars, "Stress-based nonlocal damage model," *International Journal of Solids and Structures*, vol. 48, pp. 3431–3443, 2011.
11. E. Lorentz and P. Badel, "A new path-following constraint for strain-softening finite element simulations," *International Journal for Numerical Methods in Engineering*, vol. 60, no. 2, pp. 499–526, 2004.
12. S. Silling, "Reformulation of elasticity theory for discontinuities and long-range force," *Journal of the Mechanics and Physics of Solids*, vol. 48, pp. 175–209, 2000.
13. S. Silling and E. Askari, "A meshfree method based on the peridynamic model of solid mechanics," *Computers and Structures*, vol. 83, pp. 1526–1535, 2005.
14. P. Areias, J. Reinoso, P. Camanho, and T. Rabczuk, "A constitutive-based element-by-element crack propagation algorithm with local mesh refinement," *Computational Mechanics*, vol. 56, pp. 291–315, 2015.
15. P. Areias, T. Rabczuk, and D. Dias-da-Costa, "Element-wise fracture algorithm based on rotation of edges," *Engineering Fracture Mechanics*, vol. 110, pp. 113–137, 2013.
16. Z. Yang, A. Deeks, and H. Hao, "Transient dynamic fracture analysis using scaled boundary finite element method: a frequency-domain approach," *Engineering Fracture Mechanics*, vol. 74, no. 5, pp. 669–687, 2007.
17. E. Ooi, M. Shi, C. Song, F. Tin-Loi, and Z. Yang, "Dynamic crack propagation simulation with scaled boundary polygon elements and automatic remeshing technique," *Engineering Fracture Mechanics*, vol. 106, pp. 1–21, 2013.
18. J.-H. Song, P. Areias, and T. Belytschko, "A method for dynamic crack and shear band propagation with phantom nodes," *International Journal for Numerical Methods in Engineering*, vol. 67, pp. 868–893, 2006.
19. T. Belytschko, H. Chen, J. Xu, and G. Zi, "Dynamic crack propagation based on loss of hyperbolicity with a new discontinuous enrichment," *International Journal for Numerical Methods in Engineering*, vol. 58, pp. 1873–1905, 2003.
20. Z. Wu, X. Xu, Q. Liu, and Y. Yang, "A zero-thickness cohesive element-based numerical manifold method for rock mechanical behavior with micro-voronoi grains," *Engineering Analysis with Boundary Elements*, vol. 96, pp. 94–108, 2018.
21. J. Wu and Y. Cai, "A partition of unity formulation referring to the nmm for multiple intersecting crack analysis," *Theoretical and Applied Fracture Mechanics*, vol. 72, pp. 28–36, 2014.
22. J.-Y. Wu, F.-B. Li, and S.-L. Xu, "Extended embedded finite elements with continuous displacement jumps for the modeling of localized failure in solids," *Computer Methods in Applied Mechanics and Engineering*, vol. 285, pp. 346–378, 2015.
23. F. Armero and C. Linder, "New finite elements with embedded strong discontinuities in the finite deformation range," *Computer Methods in Applied Mechanics and Engineering*, vol. 197, pp. 3138–3170, 2008.
24. T. Rabczuk and T. Belytschko, "Adaptivity for structured meshfree particle methods in 2D and 3D," *International Journal for Numerical Methods in Engineering*, vol. 63, pp. 1559–1582, 2005.
25. X. Zhuang, C. Augarde, and K. Mathisen, "Fracture modeling using meshless methods and level sets in 3D: framework and modeling," *International Journal for Numerical Methods in Engineering*, vol. 92, pp. 969–998, 2012.
26. X. Zhuang, C. Augarde, and S. Bordas, "Accurate fracture modelling using meshless methods, the visibility criterion and level sets: Formulation and 2D modelling," *International Journal for Numerical Methods in Engineering*, vol. 86, pp. 249–268, 2011.
27. P. Areias and T. Rabczuk, "Steiner-point free edge cutting of tetrahedral meshes with applications in fracture," *Finite Elements in Analysis and Design*, vol. 132, pp. 27–41, 2017.
28. P. Areias, M. Msekh, and T. Rabczuk, "Damage and fracture algorithm using the screened Poisson equation and local remeshing," *Engineering Fracture Mechanics*, vol. 158, pp. 116–143, 2016.
29. J.-Y. Wu and F.-B. Li, "An improved stable XFEM (Is-XFEM) with a novel enrichment function for the computational modeling of cohesive cracks," *Computer Methods in Applied Mechanics and Engineering*, vol. 295, pp. 77–107, 2015.
30. T. Chau-Dinh, G. Zi, P.-S. Lee, T. Rabczuk, and J.-H. Song, "Phantom-node method for shell models with arbitrary cracks," *Computers and Structures*, vol. 92-93, pp. 242–246, 2012.

31. Y. Wang, H. Waisman, and I. Harari, "Direct evaluation of stress intensity factors for curved cracks using Irwin's integral and XFEM with high-order enrichment functions," *International Journal for Numerical Methods in Engineering*, vol. 112, no. 7, pp. 629–654, 2017.
32. H. Zheng and D. Xu, "New strategies for some issues of numerical manifold method in simulation of crack propagation," *International Journal for Numerical Methods in Engineering*, vol. 97, pp. 986–1010, 2014.
33. H. Zheng, F. Liu, and X. Du, "Complementarity problem arising from static growth of multiple cracks and mls-based numerical manifold method," *Computer Methods in Applied Mechanics and Engineering*, vol. 295, pp. 150–171, 2015.
34. Z. Wu, L. Ngai, and Y. Wong, "Frictional crack initiation and propagation analysis using the numerical manifold method," *Computers and Geotechnics*, vol. 39, pp. 38–53, 2012.
35. Z. Wu, L. Fan, Q. Liu, and G. Ma, "Micro-mechanical modeling of the macro-mechanical response and fracture behavior of rock using the numerical manifold method," *Engineering Geology*, vol. 225, pp. 49–60, 2017.
36. J.-Y. Wu and V. P. Nguyen, "A length scale insensitive phase-field damage model for brittle fracture," *Journal of the Mechanics and Physics of Solids*, vol. 119, pp. 20–42, 2018.
37. J.-Y. Wu, "Robust numerical implementation of non-standard phase-field damage models for failure in solids," *Computer Methods in Applied Mechanics and Engineering*, vol. 340, pp. 767–797, 2018.
38. J.-Y. Wu, "A unified phase-field theory for the mechanics of damage and quasi-brittle failure," *Journal of the Mechanics and Physics of Solids*, vol. 103, pp. 72–99, 2017.
39. S. Zhou, X. Zhuang, H. Zhu, and T. Rabczuk, "Phase field modelling of crack propagation, branching and coalescence in rocks," *Theoretical and Applied Fracture Mechanics*, vol. 96, pp. 174–192, 2018.
40. M. Cervera, M. Chiumenti, and R. Codina, "Mixed stabilized finite element methods in nonlinear solid mechanics: Part I: Formulation," *Computer Methods in Applied Mechanics and Engineering*, vol. 199, pp. 2559–2570, 2010.
41. M. Cervera, M. Chiumenti, and R. Codina, "Mixed stabilized finite element methods in nonlinear solid mechanics: Part II: Strain localization," *Computer Methods in Applied Mechanics and Engineering*, vol. 199, pp. 2571–2589, 2010.
42. M. Cervera, M. Chiumenti, L. Benedetti, and R. Codina, "Mixed stabilized finite element methods in nonlinear solid mechanics. Part III: Compressible and incompressible plasticity," *Computer Methods in Applied Mechanics and Engineering*, vol. 285, pp. 752–775, 2015.
43. M. Cervera, M. Chiumenti, and R. Codina, "Mesh objective modeling of cracks using continuous linear strain and displacement interpolations," *International Journal for Numerical Methods in Engineering*, vol. 87, pp. 962–987, 2011.
44. M. Nikolić, E. Karavelić, A. Ibrahimbegovic, and P. Miščević, "Lattice element models and their peculiarities," *Archives of Computational Methods in Engineering*, vol. 25, pp. 753–784, Jul 2018.
45. C. Jiang, G.-F. Zhao, and N. Khalili, "On crack propagation in brittle material using the distinct lattice spring model," *International Journal of Solids and Structures*, vol. 118-119, pp. 41 – 57, 2017.
46. L. E. Kosteski, I. Iturrioz, A. P. Cisilino, R. B. D'ambra, V. Pettarin, L. Fasce, and P. Frontini, "A lattice discrete element method to model the falling-weight impact test of PMMA specimens," *International Journal of Impact Engineering*, vol. 87, pp. 120–131, 2016. SI: Experimental Testing and Computational Modeling of Dynamic Fracture.
47. G.-F. Zhao, "Developing a four-dimensional lattice spring model for mechanical responses of solids," *Computer Methods in Applied Mechanics and Engineering*, vol. 315, pp. 881–895, 2017.
48. H. Ren, X. Zhuang, Y. Cai, and T. Rabczuk, "Dual-horizon peridynamics," *International Journal for Numerical Methods in Engineering*, vol. 108, pp. 1451–1476, 2016.
49. H. Ren, X. Zhuang, and T. Rabczuk, "Dual-horizon peridynamics: A stable solution to varying horizons," *Computer Methods in Applied Mechanics and Engineering*, vol. 318, pp. 762–782, 2017.
50. V. Diana and S. Casolo, "A bond-based micropolar peridynamic model with shear deformability: Elasticity, failure properties and initial yield domains," *International Journal of Solids and Structures*, vol. 160, pp. 201 – 231, 2019.
51. H. Ren, X. Zhuang, and T. Rabczuk, "Nonlocal operator method with numerical integration for gradient solid," *Computers & Structures*, vol. 233, p. 106235, 2020.

52. S. Saloustros, M. Cervera, and L. Pelà, "Challenges, tools and applications of tracking algorithms in the numerical modelling of cracks in concrete and masonry structures," *Archives of Computational Methods in Engineering*, vol. 26, pp. 961–1005, 2019.
53. A. Alsahly, C. Callari, and G. Meschke, "An algorithm based on incompatible modes for the global tracking of strong discontinuities in shear localization analyses," *Computer Methods in Applied Mechanics and Engineering*, vol. 330, pp. 33–63, 2018.
54. Y. Zhang and X. Zhuang, "Cracking elements: a self-propagating strong discontinuity embedded approach for quasi-brittle fracture," *Finite Elements in Analysis and Design*, vol. 144, pp. 84–100, 2018.
55. Y. Zhang and X. Zhuang, "Cracking elements method for dynamic brittle fracture," *Theoretical and Applied Fracture Mechanics*, vol. 102, pp. 1–9, 2019.
56. Y. Zhang and H. A. Mang, "Global cracking elements: a novel tool for Galerkin-based approaches simulating quasi-brittle fracture," *International Journal for Numerical Methods in Engineering*, vol. 121, pp. 2462–2480, 2020.
57. L. Mu and Y. Zhang, "Cracking elements method with 6-node triangular element," *Finite Elements in Analysis and Design*, vol. 177, p. 103421, 2020.
58. D. Dias-da-Costa, J. Alfaiate, L. Sluys, P. Areias, and E. Júlio, "An embedded formulation with conforming finite elements to capture strong discontinuities," *International Journal for Numerical Methods in Engineering*, vol. 93, pp. 224–244, 2012.
59. M. Cervera, J.-Y. Wu, M. Chiumenti, and S. Kim, "Strain localization analysis of Hill's orthotropic elastoplasticity: analytical results and numerical verification," *Computational Mechanics*, vol. 65, pp. 533–554, 2020.
60. M. Nikolić, X. N. Do, A. Ibrahimbegovic, and Ž. Nikolić, "Crack propagation in dynamics by embedded strong discontinuity approach: Enhanced solid versus discrete lattice model," *Computer Methods in Applied Mechanics and Engineering*, vol. 340, pp. 480–499, 2018.
61. O. Lloberas-Valls, A. Huerta, J. Oliver, and I. Dias, "Strain injection techniques in dynamic fracture modeling," *Computer Methods in Applied Mechanics and Engineering*, vol. 308, pp. 499–534, 2016.
62. Y. Zhang, R. Lackner, M. Zeiml, and H. Mang, "Strong discontinuity embedded approach with standard SOS formulation: Element formulation, energy-based crack-tracking strategy, and validations," *Computer Methods in Applied Mechanics and Engineering*, vol. 287, pp. 335–366, 2015.
63. T. Rabczuk, S. Bordas, and G. Zi, "On three-dimensional modelling of crack growth using partition of unity methods," *Computers and Structures*, vol. 88, pp. 1391–1411, 2010.
64. T. Rabczuk and T. Belytschko, "Cracking particles: a simplified meshfree method for arbitrary evolving cracks," *International Journal for Numerical Methods in Engineering*, vol. 61, pp. 2316–2343, 2004.
65. T. Rabczuk and T. Belytschko, "A three-dimensional large deformation meshfree method for arbitrary evolving cracks," *Computer Methods in Applied Mechanics and Engineering*, vol. 196, pp. 2777–2799, 2007.
66. T. Rabczuk, G. Zi, S. Bordas, and H. Nguyen-Xuan, "A simple and robust three-dimensional cracking-particle method without enrichment," *Computer Methods in Applied Mechanics and Engineering*, vol. 199, pp. 2437–2455, 2010.
67. G. Camacho and M. Ortiz, "Computational modelling of impact damage in brittle materials," *International Journal of Solids and Structures*, vol. 33, pp. 2899–2938, 1996.
68. G. Meschke and P. Dumstorff, "Energy-based modeling of cohesive and cohesionless cracks via X-FEM," *Computer Methods in Applied Mechanics and Engineering*, vol. 196, pp. 2338–2357, 2007.
69. S. Mariani and U. Perego, "Extended finite element method for quasi-brittle fracture," *International Journal for Numerical Methods in Engineering*, vol. 58, pp. 103–126, 2003.
70. T. Belytschko, D. Organ, and C. Gerlach, "Element-free Galerkin methods for dynamic fracture in concrete," *Computer Methods in Applied Mechanics and Engineering*, vol. 187, pp. 385–399, 2000.
71. Y. Zhang and X. Zhuang, "A softening-healing law for self-healing quasi-brittle materials: analyzing with strong discontinuity embedded approach," *Engineering Fracture Mechanics*, vol. 192, pp. 290–306, 2018.
72. J. Mosler and G. Meschke, "3D modelling of strong discontinuities in elastoplastic solids: fixed and rotating localization formulations," *International Journal for Numerical Methods in Engineering*, vol. 57, pp. 1553–1576, 2003.
73. J. Mosler and O. Bruhns, "A 3D anisotropic elastoplastic-damage model using discontinuous displacement fields," *International Journal for Numerical Methods in Engineering*, vol. 60, pp. 923–948, 2004.

74. J. Simo and S. Rifai, "A class of mixed assumed strain methods and the method of incompatible modes," *International Journal for Numerical Methods in Engineering*, vol. 29, pp. 1595–1638, 1990.
75. J. Simo, J. Oliver, and F. Armero, "An analysis of strong discontinuities induced by strain-softening in rate-independent inelastic solids," *Computational Mechanics*, vol. 12, pp. 277–296, 1993.
76. J. Simo and F. Armero, "Geometrically non-linear enhanced strain mixed methods and the method of incompatible modes," *International Journal for Numerical Methods in Engineering*, vol. 33, pp. 1413–1449, 1992.
77. P. Helnwein, "Some remarks on the compressed matrix representation of symmetric second-order and fourth-order tensors," *Computer Methods in Applied Mechanics and Engineering*, vol. 190, pp. 2753–2770, 2001.
78. J. Oliver, "A consistent characteristic length for smeared cracking models," *International Journal for Numerical Methods in Engineering*, vol. 28, pp. 461–474, 1989.
79. M. Cervera and M. Chiumenti, "Smeared crack approach: back to the original track," *International Journal for Numerical and Analytical Methods in Geomechanics*, vol. 30, pp. 1173–1199, 2006.
80. S.-q. Yang, "Study of strength failure and crack coalescence behavior of sandstone containing three pre-existing fissures (in Chinese)," *Rock and Soil Mechanics (Yan Tu Li Xue)*, vol. 34, no. 1, pp. 31–39, 2013.
81. Q. Zhu, T. Ni, L. Zhao, and Y. Shuangshuang, "Simulations of crack propagation in rock-like materials using peridynamic method (in Chinese)," *Chinese Journal of Rock Mechanics and Engineering (Yan Shi Li Xue Yu Gong Cheng Xue Bao)*, vol. 35, no. s2, pp. 3507–3515, 2016.
82. D. Zhang and Q. Dong, "Fracturing and damage of 3d-Printed materials with two intermittent fissures under compression," *Materials*, vol. 13, no. 7, p. 1607, 2020.
83. H.-j. Su, H.-w. Jing, H.-h. Zhao, M.-l. Zhang, and Q. Yin, "Strength and fracture characteristic of rock mass containing parallel fissures (in Chinese)," *Engineering Mechanics (Gong Cheng Li Xue)*, vol. 32, no. 5, pp. 192–207, 2015.
84. P. Pivonka, R. Lackner, and H. A. Mang, "Shapes of loading surfaces of concrete models and their influence on the peak load and failure mode in structural analyses," *International Journal of Engineering Science*, vol. 41, no. 13, pp. 1649 – 1665, 2003.
85. T. Rabczuk and E. Samaniego, "Discontinuous modelling of shear bands using adaptive meshfree methods," *Computer Methods in Applied Mechanics and Engineering*, vol. 197, pp. 641–658, 2008.